ELSEVIER

Physica D 115 (1998) 73–86

PHYSICA D

The multiphase-field model with an integrated concept for modelling solute diffusion

J. Tiaden [a], B. Nestler [b], H.J. Diepers [a], I. Steinbach [a,*]

[a] *Access e.V. Intzestrasse 5, D-52072 Aachen, Germany*

[b] *Foundry Institute, RWTH Aachen, Intzestrasse 5, D-52072 Aachen, Germany*

Received 21 May 1997; received in revised form 1 August 1997; accepted 9 September 1997

Communicated by H. Müller-Krumbhaar

Abstract

A recent formulation of a multiphase-field model is presented. The approach is employed to numerically simulate phase transitions in multiphase systems and to describe the evolution of the microstructure during solidification processes in alloy systems. A new method for modelling solute diffusion in a binary alloy within N different phases with varying solubilities and different diffusion coefficients is integrated in the multiphase-field model. The phase-field/diffusion model derived is compared with the previous Wheeler, Boettinger and McFadden (WBM) model in a limiting case. The set of coupled evolution equations, the phase-field model equations and the concentration field equation is solved using control volume techniques on a uniform mesh. With the input of the specific phase diagram, thermophysical and materials data of the chosen real Fe–C alloy system, the multiphase-field method is successfully applied to compute the peritectic solidification process of steel. The numerical calculations of the peritectic reaction and transformation are presented. Copyright © 1998 Elsvier Science B.V.

Keywords: Phase transitions; Phase-field models; Multiphase systems; Peritectic solidification; Micro segregation; Solute diffusion

1. Introduction

The aim of the present paper is to lay out a mathematical method for modelling and numerically simulating phase transitions in multiphase systems being controlled by solute diffusion. The entire model and the corresponding set of reaction/diffusion equations are introduced in the following section. The model consists of a concept describing the solute diffusion in the whole system and its integration into the recently developed multiphase-field approach [1]. In the numerical example of Section 4, the growth process and growth rate of the crystals are limited by solute diffusion rather than by the growth kinetics.

* Corresponding author.

PII S0167-2789(97)00226-1

In several technical alloys more than two species (multiple components) might appear in the multiphase system, e.g. Al–Si–Cu, Ni-based superalloys, Y–Ba–Cu–O, etc. These even more general cases are not considered here, but may be included in future work.

Up to now the approach presented is restricted to describe binary multiphase systems. It takes stoichiometric phases as well as phases with varying solubility limits into account and allows the partition coefficients to depend on time and space. In Section 3, we treat special limiting cases of the more general form of the solute diffusion equations being discussed in Section 2. These limits enable a direct comparison with the Wheeler, Boettinger, McFadden (WBM) model for solid–liquid phase changes [2]. As an application, numerical simulations of the solidification process in the Fe–C system are presented in Section 4. The aim of these simulations is to reflect the peritectic reaction, the peritectic transformation and to study the effect and influence of the local carbon concentration on the growth behaviour and the resulting grain shapes. Conclusions are drawn in Section 5.

Phase-field models have become an attractive and useful tool for numerical and theoretical investigations of phase transitions. First order phase transitions, such as solidification in a supercooled melt, can be described well using the phase-field concept. The classical sharp interface theory leads to difficulties in the computational treatment of the free boundary problem, since the position of the interface has to be calculated explicitly. In order to handle the moving free boundary numerically, the phase-field method is used, where the interface is expressed implicitly by a time and space dependent function indicating the phase state and being defined on the whole region.

In the multiphase-field model [1], the different phases are expressed by the phase indicating functions, also called phase-field variables $\phi_\alpha(\boldsymbol{x}, t), \alpha = 1, \ldots, N$. The thicknesses of the transition layers between two phases are of the order $\eta_{\alpha\beta}$, where $\eta_{\alpha\beta}$ are small positive parameters. The relation between the multiphase-field model and a sharp interface model is shown mathematically by taking the interface thickness $\eta_{\alpha\beta}$ as zero and using matched asymptotic expansions [3,4,5]. A phase-field concept for the solidification of a pure material was studied by Collins and Levine [6] and Caginalp [7]. Kobayashi [8] and Wheeler et al. [9] developed phase-field models with anisotropic surface tensions and showed that dendritic growth into an undercooled pure melt can be simulated. Bösch et al. [10] introduced a numerical scheme of rotated and shifted lattice for solving the phase-field equations of the model by Wheeler et al. [9]. With their method they were able to remove all unphysical metastable states and to avoid any numerical anisotropy, which are both results of straight–forward discretization algorithms. Kobayashi [11] further improved this formulation to calculate dendrites in a three-dimensional space. Facetted crystal growth in a two-phase system has also been treated using the phase-field theory [12]. More recently, Gonzalez-Cinca et al. [13] presented phase-field simulations of facetted growing interfaces in a two-liquid system and they showed that the simulations reproduce qualitatively a variety of morphologies observed in the experiments.

Several phase-field models for the solidification of binary alloys have been derived with different intentions by Wheeler et al. [2] and Caginalp and Xie [14]. Recently, the coupling of the phase-field approach with fluid flow was introduced [15]. The traditional phase-field methods only distinguish between two different phases. Accordingly they only treat phase transitions in two-phase systems, e.g. a system consisting of one liquid and one solid phase. But in most alloy systems more than one phase emerges. Subsequently, Wheeler et al. [16] extended their work and introduced an additional order parameter to model the solidification of a eutectic alloy. In order to describe the more general case of phase transitions in an N-phase system, which naturally includes peritectic and eutectic systems, Steinbach et al. [1] recently proposed a particular multiphase-field approach. This method allows the simulation of growing microstructures in technically relevant alloys. Thermophysical data such as latent heat, interfacial energies, diffusion coefficients and the phase diagram data are taken into account. The local stable and metastable equilibrium temperatures between different phases that are dependent on the local solute concentration are calculated using a commercial thermodynamic database.

2. The model equations

2.1. The multiphase-field model

We consider a system of N phases and hence of N corresponding phase-field variables $\phi_1, \ldots, \phi_N$ with $0 < \phi_\alpha < 1$ for $\alpha = 1, \ldots, N$, which are functions of time and space. The N phase contributions are connected under the constraint:

$$\sum_{\beta=1}^{\beta=N} \phi_\beta = 1. \tag{1}$$

Using the approach of Steinbach et al. [1], the energy functional $\mathcal{F}$ for this system is expanded in a sum over pairwise energy differences between two phases α and β.

$$\mathcal{F}(\phi, \nabla\phi) = \int_V \sum_{\beta=1}^{\beta=N} \sum_{\alpha=1}^{\alpha=\beta} \{f_{\alpha\beta}^{\text{grad}}(\phi, \nabla\phi) + f_{\alpha\beta}^{\text{pot}}(\phi)\} \mathrm{d}V, \tag{2}$$

where $\mathcal{F}$ depends on the vector $\phi = (\phi_1, \ldots, \phi_N)$ and its gradients $\nabla\phi = (\nabla\phi_1, \ldots, \nabla\phi_N)$. The gradient and potential energy density per pair of phases α and β are

$$f_{\alpha\beta}^{\text{grad}}(\phi, \nabla\phi) = \tfrac{1}{2}\epsilon_{\alpha\beta}(\phi_\alpha \nabla\phi_\beta - \phi_\beta \nabla\phi_\alpha)^2, \tag{3}$$

$$f_{\alpha\beta}^{\text{pot}}(\phi) = \frac{1}{a_{\alpha\beta}} \phi_\alpha^2 \phi_\beta^2 - m_{\alpha\beta} \left(\frac{1}{3}\phi_\alpha^3 + \phi_\alpha^2 \phi_\beta - \frac{1}{3}\phi_\beta^3 - \phi_\beta^2 \phi_\alpha \right). \tag{4}$$

$\epsilon_{\alpha\beta}$ is the gradient energy coefficient and $1/a_{\alpha\beta}$ is the proportional to the pairwise energy barrier height. The driving force for the phase transition between the phases α and β is defined by the deviation from the two phase equilibrium. It depends on the local concentration and temperature and is described by $m_{\alpha\beta} = m_{\alpha\beta}(c, T)$. The coefficients obey the symmetry relations:

$$\epsilon_{\alpha\beta} = \epsilon_{\beta\alpha}, \quad a_{\alpha\beta} = a_{\beta\alpha}, \quad m_{\alpha\beta} = -m_{\beta\alpha}. \tag{5}$$

Formally the model allows $\binom{N}{2}$ driving forces $m_{\alpha\beta}$ for all pairs of phases to be specified. They must be derived from the N free energy levels, e.g. $\mathcal{F}^{\text{cv}}_{\alpha\equiv 1, \beta\equiv 0}$ with $\beta = 1, \ldots, N$ and $\beta \neq \alpha$, of the N pure and uniform systems, where $\mathcal{F}^{\text{cv}}$ is the free energy functional $\mathcal{F}$ restricted to the local control volume cv:

$$m_{\alpha\beta} = (\mathcal{F}^{\text{cv}}_{\alpha\equiv 1, \beta\equiv 0} - \mathcal{F}^{\text{cv}}_{\alpha\equiv 0, \beta\equiv 1}) N^{-1}, \tag{6}$$

N is the appropriate normalization:

$$N = \frac{3}{2} \int_{V^{\text{cv}}} \mathrm{d}V.$$

The driving forces correspond to the transitions between the individual energy levels of the different phases. The situation is depicted in Fig. 1.

The energy levels $\mathcal{F}^{\text{cv}}_{\alpha\equiv 1, \beta\equiv 0}$ of the bulk phases depend on the local concentration and temperature. Their exact specification is introduced in Section 4.

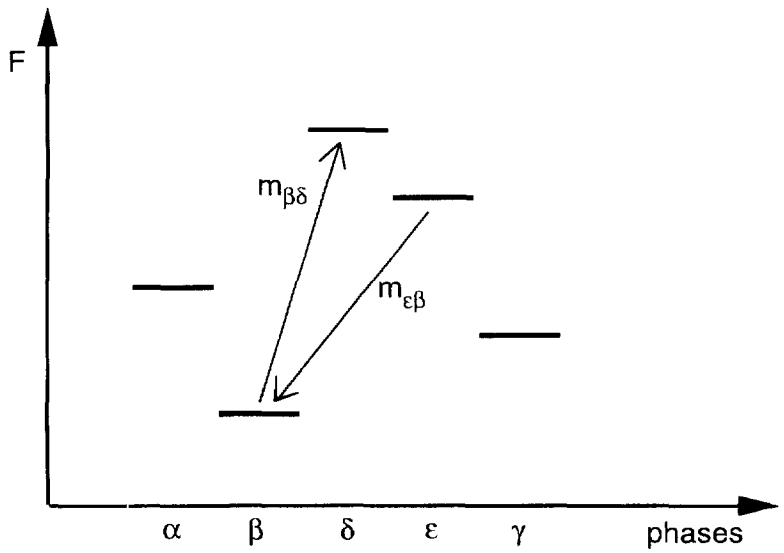

Fig. 1. The schematic drawing outlines possible transitions between energy levels corresponding to different phases in the system.

The equations of motion for the N individual phases are derived by minimizing the free energy functional, Eq. 2, with respect to the individual phases in the system (for details see [1]):

$$\dot{\phi}_\alpha = \sum_{\beta\neq\alpha}^{N} \frac{1}{\tau_{\alpha\beta}} \left(\nabla \frac{\partial}{\partial \nabla \phi_\alpha} - \frac{\partial}{\partial \phi_\alpha} \right) (f_{\alpha\beta}^{\text{grad}} + f_{\alpha\beta}^{\text{pot}})$$

$$= \sum_{\beta\neq\alpha}^{N} \frac{1}{\tau_{\alpha\beta}} \left[\epsilon_{\alpha\beta} (\phi_\alpha \nabla^2 \dot{\phi}_\beta - \phi_\beta \nabla^2 \phi_\alpha) - \frac{\phi_\alpha \phi_\beta}{2a_{\alpha\beta}} (\phi_\beta - \phi_\alpha - 2m_{\alpha\beta}) \right]. \tag{7}$$

Expression (7) holds for isotropic systems. It is straightforward to further extend the concept for anisotropic systems. The specific feature of the set of differential Eq. (7) is its ability to describe multiple phase points in a system of N phases, to take different physical properties of all N phases into account.

Numerical calculations have shown that in the general asymmetric case $\epsilon_{\alpha\beta} \neq \epsilon_{\alpha\gamma}$ the force balance at a triple junction, according to Young's law, is not reproduced. This is due to the fact that only pairwise interaction terms in the derivation of Eq. 7 are considered. Thus we restrict ourselves to the symmetric situation $\epsilon_{\alpha\beta} = \epsilon_{\alpha\gamma}$ as the asymmetric case is of minor importance for the aims of this paper and for the applications below. Rigorous analytical treatment of the multiphase model including higher order terms (f^{grad}, f^{pot} depending on more than two phases) shows that in the sharp interface limit the force balance is also achieved for the asymmetric case and will be published elsewhere [5].

2.2. *The solute diffusion equation for binary systems*

The N phase-field variables of the system may be ordered in such a way that the first n phase-fields $\phi_1, \ldots, \phi_n$ represent n phases with finite solubility limits and the next $N - n$ phase-fields $\phi_{n+1}^{\text{st}}, \ldots, \phi_N^{\text{st}}$ describe all residual stoichiometric phases in the system. The mixture concentration $c(\boldsymbol{x}, t)$ is defined by

$$c(\boldsymbol{x},t)=\sum_{\gamma=1}^{N}\phi_\gamma c_\gamma, \tag{8}$$

where $c_\gamma(\boldsymbol{x},t)$ is the concentration of one component in the phase γ of the binary alloy depending on time and space. Using the notation c_β^{st} for the concentration of the component in the stoichiometric phase β, the sum can be split into two parts, one for the phases with varying solubility limits and one for the stoichiometric phases. The expression above can be rewritten

$$c(\boldsymbol{x},t)=\sum_{\alpha=1}^{n}\phi_\alpha c_\alpha+\sum_{\beta=n+1}^{N}\phi_\beta^{\mathrm{st}}c_\beta^{\mathrm{st}}=\sum_{\alpha=1}^{n}\phi_\alpha k_{\alpha\Lambda}c_\Lambda+\sum_{\beta=n+1}^{N}\phi_\beta^{\mathrm{st}}c_\beta^{\mathrm{st}}. \tag{9}$$

Here we assume that the partition relation holds, since the first n phases are non-stoichiometric

$$c_\alpha=k(c_\alpha^*(T),c_\Lambda^*(T))c_\Lambda=k_{\alpha\Lambda}c_\Lambda, \tag{10}$$

where c_Λ is a reference concentration in phase Λ chosen arbitrarily, but with a non-vanishing phase contribution $\phi_\Lambda>0$. The $k_{\alpha\Lambda}$ are the partition coefficients being deduced from the specific equilibrium phase diagram, including its metastable extensions.

Based on the ideas of the volume averaging method, we take the following general approach for modelling solute diffusion in the system of N phases with different diffusion coefficients D_α, $\alpha=1,\ldots,n$ or D_β^{st}, $\beta=n+1,\ldots,N$, respectively,

$$\dot{c}(\boldsymbol{x},t)=\nabla\left\{\sum_{\gamma=1}^{N}\phi_\gamma D_\gamma\nabla c_\gamma\right\}=\nabla\left\{\sum_{\alpha=1}^{n}\phi_\alpha D_\alpha\nabla(k_{\alpha\Lambda}c_\Lambda)\right\}+\nabla\left\{\sum_{\beta=n+1}^{N}\phi_\beta^{\mathrm{st}}D_\beta^{\mathrm{st}}\nabla c_\beta^{\mathrm{st}}\right\}, \tag{11}$$

where $\phi_\gamma D_\gamma\nabla c_\gamma$ is the diffusive flux of the concentration within the phase γ with the local density ϕ_γ. The approach (11) is based on the physical statement that the mixture concentration c in an infinitesimally small volume or in the finite control volume of the numerical model can only change by external fluxes over the boundary of this volume. These fluxes are superposed according to the local phase densities ϕ_γ which have to be evaluated on the boundary of the volume.

Using $\nabla c_\beta^{\mathrm{st}}=0$ and substituting Eq. (9), the last expression becomes

$$\dot{c}(\boldsymbol{x},t)=\nabla\left\{\sum_{\alpha=1}^{n}\phi_\alpha D_\alpha\nabla\left(\frac{k_{\alpha\Lambda}(c-\sum_{\beta=n+1}^{N}\phi_\beta^{\mathrm{st}}c_\beta^{\mathrm{st}})}{\sum_{\delta=1}^{n}\phi_\delta k_{\delta\Lambda}}\right)\right\}$$

$$=\nabla\left\{\sum_{\alpha=1}^{n}\phi_\alpha D_\alpha\nabla\left(\frac{k_{\alpha\Lambda}c}{\sum_{\delta=1}^{n}\phi_\delta k_{\delta\Lambda}}\right)\right\}-\nabla\left\{\sum_{\alpha=1}^{n}\phi_\alpha D_\alpha\nabla\left(k_{\alpha\Lambda}\frac{\sum_{\beta=n+1}^{N}\phi_\beta^{\mathrm{st}}c_\beta^{\mathrm{st}}}{\sum_{\delta=1}^{n}\phi_\delta k_{\delta\Lambda}}\right)\right\}.$$

Assuming that the partition coefficients in general not only depend on time but also on space $k_{\alpha\Lambda}=k_{\alpha\Lambda}(\boldsymbol{x},t)$, a calculation gives the general form of the solute diffusion equation

$$\dot{c}(\boldsymbol{x},t)=\nabla\left\{\frac{\sum_{\alpha=1}^{n}\phi_\alpha D_\alpha k_{\alpha\Lambda}}{\sum_{\delta=1}^{n}\phi_\delta k_{\delta\Lambda}}\left[\nabla c-\frac{c}{\sum_{\delta=1}^{n}\phi_\delta k_{\delta\Lambda}}\left(\sum_{\delta=1}^{n}k_{\delta\Lambda}\nabla\phi_\delta+\phi_\delta\nabla k_{\delta\Lambda}\right)\right]\right.$$

$$\left.+\frac{\sum_{\alpha=1}^{n}\phi_\alpha D_\alpha c\nabla k_{\alpha\Lambda}}{\sum_{\delta=1}^{n}\phi_\delta k_{\delta\Lambda}}\right\}$$

$$- \nabla \left\{ \frac{\sum_{\alpha=1}^{n} \phi_\alpha D_\alpha}{\sum_{\delta=1}^{n} \phi_\delta k_{\delta\Lambda}} \left[\sum_{\beta=n+1}^{N} (\phi_\beta^{\mathrm{st}} \nabla k_{\alpha\Lambda} + k_{\alpha\Lambda} \nabla \phi_\beta^{\mathrm{st}}) c_\beta^{\mathrm{st}} \right.\right.$$
$$\left.\left. - \frac{k_{\alpha\Lambda} \sum_{\beta=n+1}^{N} \phi_\beta^{\mathrm{st}} c_\beta^{\mathrm{st}}}{\sum_{\delta=1}^{n} \phi_\delta k_{\delta\Lambda}} \left(\sum_{\delta=1}^{n} k_{\delta\Lambda} \nabla \phi_\delta + \phi_\delta \nabla k_{\delta\Lambda} \right) \right] \right\}. \tag{12}$$

3. Limiting cases and discussion of the derived model

3.1. Reduction to a solid/liquid interface model

Some applications of the diffusion equation derived above are now considered. In the following, the assumptions resulting from the special multiphase system selected simplify the parabolic differential Eq. (12).

- Assuming a system of N phases and the absence of any pure stoichiometric phases, the equation reduces to

$$\dot{c}(\boldsymbol{x}, t) = \nabla \left\{ \frac{\sum_{\alpha=1}^{N} \phi_\alpha D_\alpha k_{\alpha\Lambda}}{\sum_{\delta=1}^{N} \phi_\delta k_{\delta\Lambda}} \left[\nabla c - \frac{c}{\sum_{\delta=1}^{N} \phi_\delta k_{\delta\Lambda}} \left(\sum_{\delta=1}^{N} k_{\delta\Lambda} \nabla \phi_\delta + \phi_\delta \nabla k_{\delta\Lambda} \right) \right] \right.$$
$$\left. + \frac{\sum_{\alpha=1}^{N} \phi_\alpha D_\alpha c \nabla k_{\alpha\Lambda}}{\sum_{\delta=1}^{N} \phi_\delta k_{\delta\Lambda}} \right\}. \tag{13}$$

- Restricting the system moreover to the presence of only two phases, we choose a solid–liquid interface and we call the parameters ϕ_s, D_s, c_s and ϕ_l, D_l, c_l for the solid and liquid phases, respectively. The partition relation is $c_\mathrm{s} = k_{\mathrm{sl}} c_\mathrm{l}$ where the partition coefficient k_{sl} still depends on space. Using the constraint $\phi_\mathrm{l} + \phi_\mathrm{s} = 1$ and having the restriction that both solid and liquid are phases with varying solubilities we get

$$\begin{aligned}
\dot{c}(\boldsymbol{x}, t) &= \nabla \{ \phi_\mathrm{l} D_\mathrm{l} \nabla c_\mathrm{l} + \phi_\mathrm{s} D_\mathrm{s} \nabla c_\mathrm{s} \} \\
&= \nabla \{ \phi_\mathrm{l} D_\mathrm{l} \nabla c_\mathrm{l} + \phi_\mathrm{s} D_\mathrm{s} \nabla (k_{\mathrm{sl}} c_\mathrm{l}) \} \\
&= \nabla \left\{ \phi_\mathrm{l} D_\mathrm{l} \nabla \left(\frac{c}{\phi_\mathrm{l} + k_{\mathrm{sl}} \phi_\mathrm{s}} \right) + \phi_\mathrm{s} D_\mathrm{s} \nabla \left(\frac{k_{\mathrm{sl}} c}{\phi_\mathrm{l} + k_{\mathrm{sl}} \phi_\mathrm{s}} \right) \right\} \\
&= \nabla \left\{ (1 - \phi_\mathrm{s}) D_\mathrm{l} \nabla \left(\frac{c}{1 + \phi_\mathrm{s}(k_{\mathrm{sl}} - 1)} \right) + \phi_\mathrm{s} D_\mathrm{s} \nabla \left(\frac{k_{\mathrm{sl}} c}{1 + \phi_\mathrm{s}(k_{\mathrm{sl}} - 1)} \right) \right\}.
\end{aligned}$$

A calculation gives

$$\dot{c}(\boldsymbol{x}, t) = \nabla \left\{ \frac{D_\mathrm{l}(1 + \phi_\mathrm{s}((D_\mathrm{s}/D_\mathrm{l}) k_{\mathrm{sl}} - 1))}{1 + \phi_\mathrm{s}(k_{\mathrm{sl}} - 1)} \left[\nabla c - \frac{c(k_{\mathrm{sl}} - 1)}{1 + \phi_\mathrm{s}(k_{\mathrm{sl}} - 1)} \nabla \phi_\mathrm{s} \right] \right.$$
$$\left. + \frac{\phi_\mathrm{s} c}{1 + \phi_\mathrm{s}(k_{\mathrm{sl}} - 1)} \left[D_\mathrm{s} - \frac{D_\mathrm{l}(1 + \phi_\mathrm{s}(\frac{D_\mathrm{s}}{D_\mathrm{l}} k_{\mathrm{sl}} - 1))}{1 + \phi_\mathrm{s}(k_{\mathrm{sl}} - 1)} \right] \nabla k_{\mathrm{sl}} \right\}$$
$$\dot{c}(\boldsymbol{x}, t) = \nabla \left\{ D^* \left[\nabla c - \frac{c(k_{\mathrm{sl}} - 1)}{1 + \phi_\mathrm{s}(k_{\mathrm{sl}} - 1)} \nabla \phi_\mathrm{s} \right] + \frac{\phi_\mathrm{s} c}{1 + \phi_\mathrm{s}(k_{\mathrm{sl}} - 1)} (D_\mathrm{s} - D^*) \nabla k_{\mathrm{sl}} \right\}, \tag{14}$$

where we defined

$$D^* := \frac{D_\mathrm{l}(1 + \phi_\mathrm{s}((D_\mathrm{s}/D_\mathrm{l}) k_{\mathrm{sl}} - 1))}{1 + \phi_\mathrm{s}(k_{\mathrm{sl}} - 1)}. \tag{15}$$

– Assuming the partition coeffcient k_{sl} does not depend on space, the equation for the solid–liquid interface reduces to

$$\dot{c}(\boldsymbol{x}, t) = \nabla \left\{ D^* \left[\nabla c - \frac{c(k_{sl} - 1)}{1 + \phi_s(k_{sl} - 1)} \nabla \phi_s \right] \right\}, \tag{16}$$

since ∇k_{sl} vanishes. At this stage, we introduce a rewritten expression for $\dot{c}(\boldsymbol{x}, t)$ which will be referred to in Section 3.2 where we compare our model with the WBM concept

$$\dot{c}(\boldsymbol{x}, t) = \nabla\{D^*[\nabla c - (c_l k_{sl} - c_l)\nabla\phi_s]\} = \nabla\{D^*[\nabla c + (c_l - c_s)\nabla\phi_s]\}, \tag{17}$$

where we used

$$c = c_l\phi_l + c_s\phi_s = c_l\phi_l + \phi_s k_{sl} c_l.$$

– Finally, an equation for the rate of change of the concentration in the liquid with time $\dot{c}_l$, still working in a solid/liquid system, is derived even considering the partition coefficient to depend on time $k_{sl} = k_{sl}(\boldsymbol{x}, t)$. Using the implication $\dot{\phi}_l = -\dot{\phi}_s$ of constraint (1) and the partition relation $c_s = k_{sl} c_l$ we can write

$$\begin{aligned} \dot{c}(\boldsymbol{x}, t) &= \dot{c}_l\phi_l + c_l\dot{\phi}_l + \dot{c}_s\phi_s + \dot{\phi}_s c_s \\ &= \dot{c}_l(1 - \phi_s) - c_l\dot{\phi}_s + \dot{k}_{sl} c_l\phi_s + k_{sl}\dot{c}_l\phi_s + k_{sl} c_l\dot{\phi}_s. \end{aligned} \tag{18}$$

Applying approach (11) we get

$$\begin{aligned} &\dot{c}_l(1 - \phi_s) - c_l\dot{\phi}_s + \dot{k}_{sl} c_l\phi_s + k_{sl}\dot{c}_l\phi_s + k_{sl} c_l\dot{\phi}_s \\ &= \nabla\{\phi_l D_l \nabla c_l + \phi_s D_s c_l \nabla k_{sl} + \phi_s D_s k_{sl} \nabla c_l\} \\ &= \nabla\{(D_l + \phi_s(k_{sl} D_s - D_l))\nabla c_l + \phi_s D_s c_l \nabla k_{sl}\} \\ &= \nabla \left\{ D_l \left(1 + \phi_s \left(\frac{D_s}{D_l} k_{sl} - 1 \right) \right) \nabla c_l + \phi_s D_s c_l \nabla k_{sl} \right\}. \end{aligned} \tag{19}$$

From rearranging, it follows that

$$\begin{aligned} \dot{c}_l = &\frac{1}{1 + \phi_s(k_{sl} - 1)} \nabla \left\{ D_l \left(1 + \phi_s \left(\frac{D_s}{D_l} k_{sl} - 1 \right) \right) \nabla c_l + \phi_s D_s c_l \nabla k_{sl} \right\} \\ &+ \frac{1}{1 + \phi_s(k_{sl} - 1)} ((1 - k_{sl}) c_l \dot{\phi}_s - \dot{k}_{sl} c_l \phi_s). \end{aligned} \tag{20}$$

– If k_{sl} does not depend on t and $\boldsymbol{x}$ we get

$$\dot{c}_l = \frac{1}{1 + \phi_s(k_{sl} - 1)} \left[\nabla \left\{ D_l \left(1 + \phi_s \left(\frac{D_s}{D_l} k_{sl} - 1 \right) \right) \nabla c_l \right\} + (1 - k_{sl}) c_l \dot{\phi}_s \right]. \tag{21}$$

– The multiphase-field equation in the liquid/solid case reduces to the standard form by inserting $\phi_l = 1 - \phi_s$:

$$\tau\dot{\phi}_s = \epsilon\nabla^2\phi_s + \frac{1}{a}\phi_s(1 - \phi_s)\left(\frac{1}{2} - \phi_s\right) + m\phi_s(1 - \phi_s). \tag{22}$$

3.2. *Coupling of the multiphase-field with the solute diffusion equations*

The coupling of the multiphase-field with the solute diffusion equations has to be considered in two ways. The coupling direction $\phi \rightarrow c$ thereby arises naturally from Eq. (12). For each configuration $\phi_\alpha(\boldsymbol{x}, t)$, the mixture

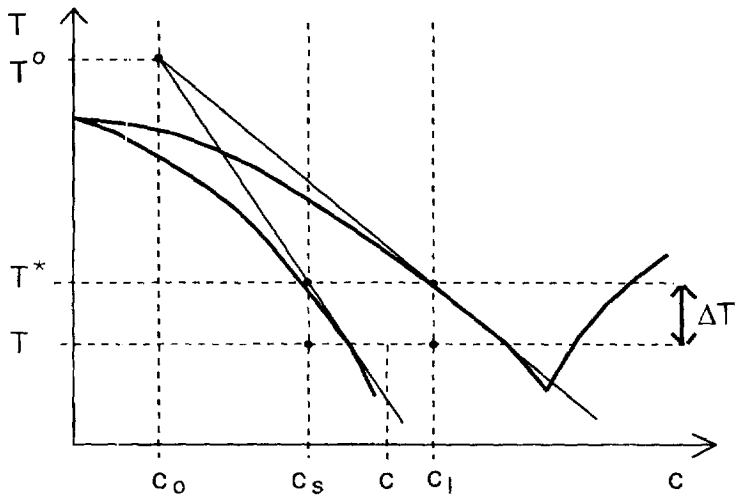

Fig. 2. Local linearization of a schematic eutectic phase diagram.

concentration $c(\boldsymbol{x}, t)$ has a distinct equilibrium solution. The transient solutions depend on the time dependent distribution of the $\phi_\alpha(\boldsymbol{x}, t)$ implicitly. There is no explicit source term of the form $\chi\dot{\phi}$ with an appropriate coupling constant χ. Such a source arises if the mixture concentration field Eq. (12) is split into an equation for c_l or c_s, respectively, Eq. (21). The source term

$$\chi\dot{\phi}_\mathrm{s} = \frac{1}{1+\phi_\mathrm{s}(k_\mathrm{sl}-1)}\nabla(1-k_\mathrm{sl})c_\mathrm{s}\dot{\phi}_\mathrm{s} \tag{23}$$

in Eq. (21) for the liquid concentration corresponds to a sink term $\tilde{\chi}\dot{\phi}_\mathrm{s}$ in the congruent equation for the solid concentration.

The reverse direction of coupling $c \to \phi$ is described by Eq. (6). For the solutal solid/liquid system, we have to specify the free energy difference $\mathcal{F}_\mathrm{l}^\mathrm{cv} - \mathcal{F}_\mathrm{s}^\mathrm{cv}$ depending on the local mixture concentration and on the local order parameter ϕ_s. While this can be done in general using a thermodynamical approach, a pragmatic way is to use the local linearization of the metastable phase diagram, Fig. 2.

For an order parameter ϕ_s and a mixture concentration c the local equilibrium temperature $T^*(c, \phi_\mathrm{s})$ is in linear approximation given by

$$T^*(c, \phi_\mathrm{s}) = T^*(c_\mathrm{l}) = T^*\left(\frac{c}{1-\phi_\mathrm{s}-k_\mathrm{sl}\phi_\mathrm{s}}\right) = T^0 + m(c_\mathrm{l} - c_0), \tag{24}$$

where T^0 and c^0 are the temperature and concentration at the intersection of the linearized solidus and liquidus lines corresponding to the local mixture concentration c and the temperature T, Fig. 2. The free energy difference is then defined in the standard way by the latent heat L and the undercooling

$$\mathcal{F}_\mathrm{s}^\mathrm{cv} - \mathcal{F}_\mathrm{l}^\mathrm{cv} = \Delta S_\mathrm{f}^\mathrm{cv}(T - T^*), \tag{25}$$

where $\Delta S_\mathrm{f}^\mathrm{cv}$ is the entropy of fusion.

3.3. Comparison with the Wheeler, Boettinger and McFadden model

In the isothermal case and neglecting surface anisotropy, the model equations for the phase-field variable and for the concentration field of Wheeler [2] are given by

$$\frac{\partial \phi_s}{\partial t} = M_1 \left\{ \epsilon^2 \nabla^2 \phi_s - \frac{\partial f}{\partial \phi_s} \right\}$$
$$= M_1 \{ \epsilon^2 \nabla^2 \phi_s - cW_B[\phi_s(\phi_s - 1)(\phi_s - \tfrac{1}{2} - \beta_B(T))]$$
$$- (1-c) W_A[\phi_s(\phi_s - 1)(\phi_s - \tfrac{1}{2} - \beta_A(T))] \} \tag{26}$$

$$\frac{\partial c}{\partial t} = M_2 \nabla \left\{ c(1-c) \nabla \frac{\partial f}{\partial c} \right\} = M_2 \nabla \left\{ \frac{RT}{v_m} \nabla c + c(1-c) \nabla (f_B - f_A) \right\}, \tag{27}$$

where the notation convention is taken from the original paper of Wheeler et al. [2] with $\phi = \phi_s$. Eq. (27) may be reformulated to

$$\frac{\partial c}{\partial t} = M_2 \nabla \left\{ \frac{RT}{v_m} \nabla c + c(1-c) \left[\frac{\partial}{\partial \phi_s} (f_B - f_A) \right] \nabla \phi_s \right\}$$
$$= M_2 \nabla \left\{ \frac{RT}{v_m} \nabla c + \tilde{M}(c, \phi_s) \nabla \phi_s \right\}, \tag{28}$$

where

$$\tilde{M}(c, \phi_s) = c(1-c) \left[\frac{\partial}{\partial \phi_s} (f_B - f_A) \right]. \tag{29}$$

This equation has the same structure as Eq. 17 of our presented model. Using thermodynamical arguments, see e.g. [17], $\tilde{M}$ can be set into proportionality with the difference between c_s and c_l. This difference is used in our formulation as a given quantity from the specific phase diagram, while it is incorporated into the model by Wheeler et al. .

The phase-field equation (26) can be rewritten to

$$\frac{\partial \phi_s}{\partial t} = M_1 \{ \epsilon^2 \nabla^2 \phi_s - [cW_B + (1-c)W_A] \phi_s(\phi_s - 1)(\phi_s - \tfrac{1}{2})$$
$$+ \phi_s(\phi_s - 1)[cW_B \beta_B + (1-c) W_A \beta_A] \}$$
$$= M_1 \{ \epsilon^2 \nabla^2 \phi_s - W'(\phi_s) + g(\phi_s)(c - c^*) \}, \tag{30}$$

where we introduced the derivative of the potential

$$W'(\phi_s) = [cW_B + (1-c)W_A] \varphi_s(\phi_s - 1)(\phi_s - \tfrac{1}{2}), \tag{31}$$

the coupling function

$$g(\phi_s) = \phi_s(\phi_s - 1)(W_B \beta_B - W_A \beta_A) \quad \text{and} \quad c^* = \frac{W_A \beta_A}{W_A \beta_A - W_B \beta_B}$$

as a measure of the mean interface concentration. In a specific phase diagram c^* describes the mid (equalG) line between solidus and liquidus concentration.

The most striking difference with respect to our formulation in Eq. (22) is the definition of the driving force. In the WBM-formulation, it is proportional to $(c - c^*)$ which is a strongly varying function over the phase boundary. Eq. (26) can be rearranged to

$$\frac{\partial \phi_s}{\partial t} = M_1 \{ \epsilon^2 \nabla^2 \phi_s - W'(\phi_s) + g(\phi_s)(c^{eq} - c^*(T)) + g(\phi_s)(c - c^{eq}) \}, \tag{32}$$

where we introduced the "equilibrium" distribution c^{eq} (that is in general unknown) in such a way that $(c - c^*(T))$ is split into one part proportional to $(c - c^{eq})$ vanishing in equilibrium and into another part proportional to $(c^{eq} - c^*(T))$.

Since $c^*(T)$ is a function of the temperature and only weakly varying in space, while c and c^{eq} strongly vary over the phase boundary, $(c^{eq} - c^*(T))$ does not vanish in equilibrium. Thus, it contributes to the equilibrium solution and influences the interface thickness and the Gibbs–Thomson relation. Therefore to our present understanding the correspondence of the phase-field parameters ϵ and W' to the physical parameters η and σ has in general a contribution that depends on the solution of c and ϕ.

To conclude, we find the model presented and the WBM-model to be equivalent in special limiting cases. Whilst the importance of the WBM-model lies in the thermodynamic consistent derivation, the model presented can easily be motivated and is more flexible regarding the identification of the model parameters to specific phase diagrams.

4. Application to peritectic solidification processes in the Fe–C system

Investigating the solidification of steel Fe–C in binary approximation, the solid phases are non-stoichiometric. It is well known that the solid state diffusion of carbon in steel cannot be neglected. It plays an important role during the peritectic transformation due to the high diffusivity of carbon. The fundamental mechanisms of the peritectic transition in Fe–C are reproduced well by coupling the diffusion equation for the mixture concentration with the phase-field equations [18].

The influence of carbon diffusion on the peritectic transformation is studied in first simulations in one spatial dimension, Fig. 3.

We assumed a planar solidification front situated in an isolated melt as the initial condition. Starting from the melting temperature, the whole system is continuously cooled down with a cooling rate of 0.5 K/s. The propagation of the different phasefields during the cooling process is shown at five different temperatures. The diffuse interface regions between any pair of phases are marked with black lines. The first three temperature steps at 1781, 1776 and 1766 K consider the growth process of the properitectic δ-ferrite phase. The curves in the first diagram reflect the distribution of carbon at these temperatures. The melt has an initial carbon concentration of 0.3 wt% and the δ-ferrite phase is in equilibrium at a concentration of 0.0577 wt%. The carbon concentration in the melt rapidly increases during the growth of δ-ferrite due to the lower solubility of the δ-ferrite phase. The amount of carbon in the ferrite at the phase boundary to the liquid always tends to adjust the equilibrium melt carbon concentration.

The last two temperature steps 1764 and 1759 K illustrate the peritectic transformation. Below the peritectic temperature, the peritectic γ-austenite phase nucleates on the properitectic δ-ferrite phase. γ-austenite grows under simultaneous dissolution of δ-ferrite and of the liquid. The peritectic transformation is controlled by the solid diffusion of carbon through the γ-austenite. The appropriate concentration profile is drawn in the second diagram and the expected concentration gradient in the austenite phase can be seen well. This gradient causes continuous carbon transport through the austenite layer so that the peritectic transformation takes place without immediate contact between the ferrite and the melt.

Two-dimensional numerical calculations were carried out as the next aim. In addition to thermodynamical and kinetic forces, the model also considers the effect of curvature. The parameters for the simulations are $c_0 = 0.3\,\text{wt\%}$, $\dot{T} = 0.5\,\text{K/s}$, $D_L = 3 \times 10^{-5}\,\text{cm}^2/\text{s}$, $D_\delta = 6 \times 10^{-6}\,\text{cm}^2/\text{s}$, $D_r = 10^{-6}\,\text{cm}^2/\text{s}$. Since no specific values for the austenite/ferrite interfacial energies are known, we chose $\sigma_{\gamma\delta} = \sigma_{L\gamma} = \sigma_{L\delta} = 2.04 \times 10^{-4}\,\text{J/cm}^2$. Thermodynamical parameters are taken from the metastable phase diagram of Fe–C depicted in Fig. 4. A grid of 150×150 cells with a spacing of 2 μm and a time step of $\Delta t = 5 \times 10^{-4}$ s are used and periodical boundary conditions are applied. The simulations took about two days CPU time on a single processor of a silicon graphics power challenge.

The numerical calculation, Fig. 5, presents the evolution of the carbon concentration field. Below the peritectic temperature, single austenite nuclei are set arbitrarily onto the four ferrite/liquid interfaces. In general, this could be done if critical nucleation undercooling is exceeded locally. This critical nucleation undercooling could be a

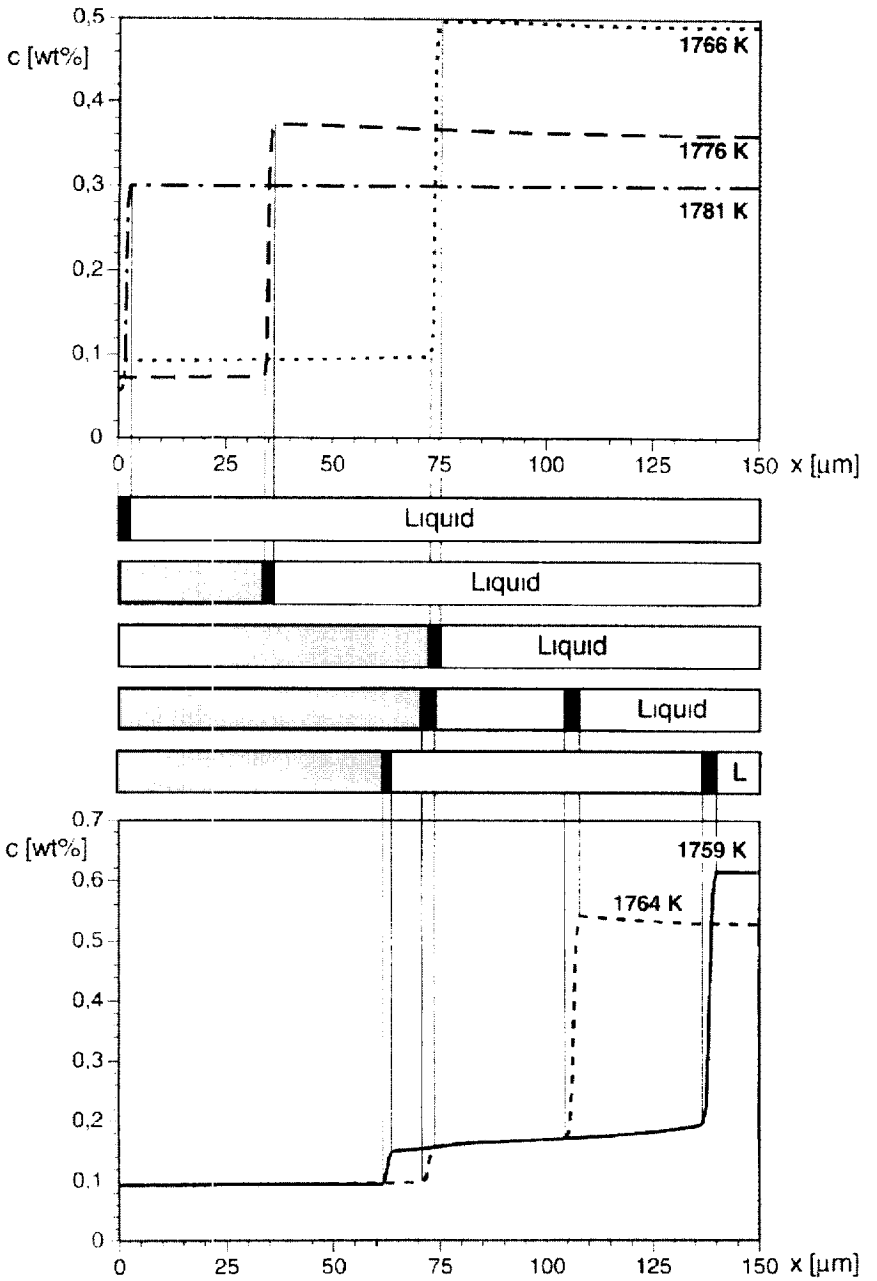

Fig. 3. The one-dimensional growth of the properitectic δ-ferrite phase and the subsequent peritectic transformation is simulated using the coupled phase-field/diffusion model. The appropriate concentration profiles are shown at different temperatures.

fixed value or could obey some statistical distribution. In both cases a new nucleus will, in a certain surrounding, reduce the undercooling and thereby limit the effective grain density [19]. The distances of the ferrite/austenite particles are chosen of the order of typical secondary dendrite arm spacings. Now the temperature of the whole system is decreased continuously by a constant cooling rate $\dot{T}$. Although the carbon distribution in the liquid is

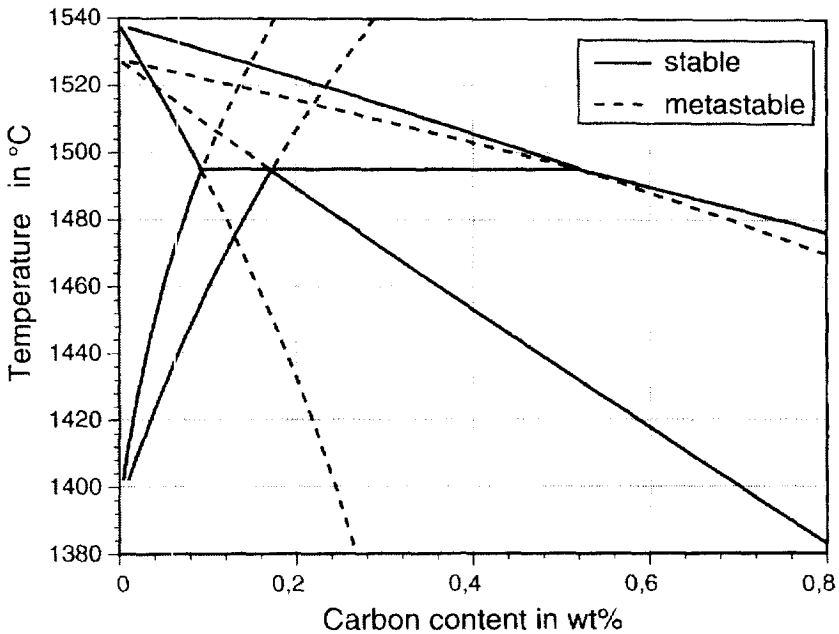

Fig. 4. Fe–C phase diagram including metastable extensions.

nearly homogeneous, the four ferrite/austenite grains interact and influence each other due to the far-reaching concentration fields. At the triplepoints, the three phases ferrite/austenite and liquid coexist and react in direct contact in a peritectic reaction. The peritectic austenite phase grows around the primary properitectic ferrite phase by a simultaneous consumption of both the ferrite and the liquid. As the austenite isolates the ferrite from the liquid and the ferrite is completely enclosed by the austenite, the austenite/liquid interface becomes separated from the austenite/ferrite interface. In order to calculate the driving force for the austenite/ferrite transition, the equilibrium conditions are taken from the metastable phase diagram, Fig. 4.

Below the peritectic temperature range, the ferrite is not a stable phase. As the carbon content of the austenite at the interface to the liquid is higher than the carbon content at the metastable interface to the ferrite, a concentration gradient is established in the austenite layer. This gradient causes solid state diffusion of carbon from the liquid to the ferrite and enables the further growth of the austenite. The so-called peritectic transformation continues by the carbon diffusion through the solid austenite phase.

5. Conclusion

A phase-field method for solutal driven phase transitions in binary multiphase systems was established. The solute diffusion model is based on the superposition of individual fluxes of species in different phases. The concentrations of the species are assumed to be connected by equilibrium partitions at phase boundaries and triplejunctions. In general, the model allows more than three phases to be present in the whole system. According to Gibb's phase rule, only the situation of triplejunctions can exist locally. The driving forces for the phase change $\dot{\phi}_\alpha$ are defined by the deviation of the local concentrations within the different phases from the metastable phase diagram.

The applications to peritectic solidification of Fe–C under realistic conditions and to a eutectic alloy [20] demonstrate the general applicability of the model. Further work will be addressed to the extension of the model presented to consider multicomponent systems.

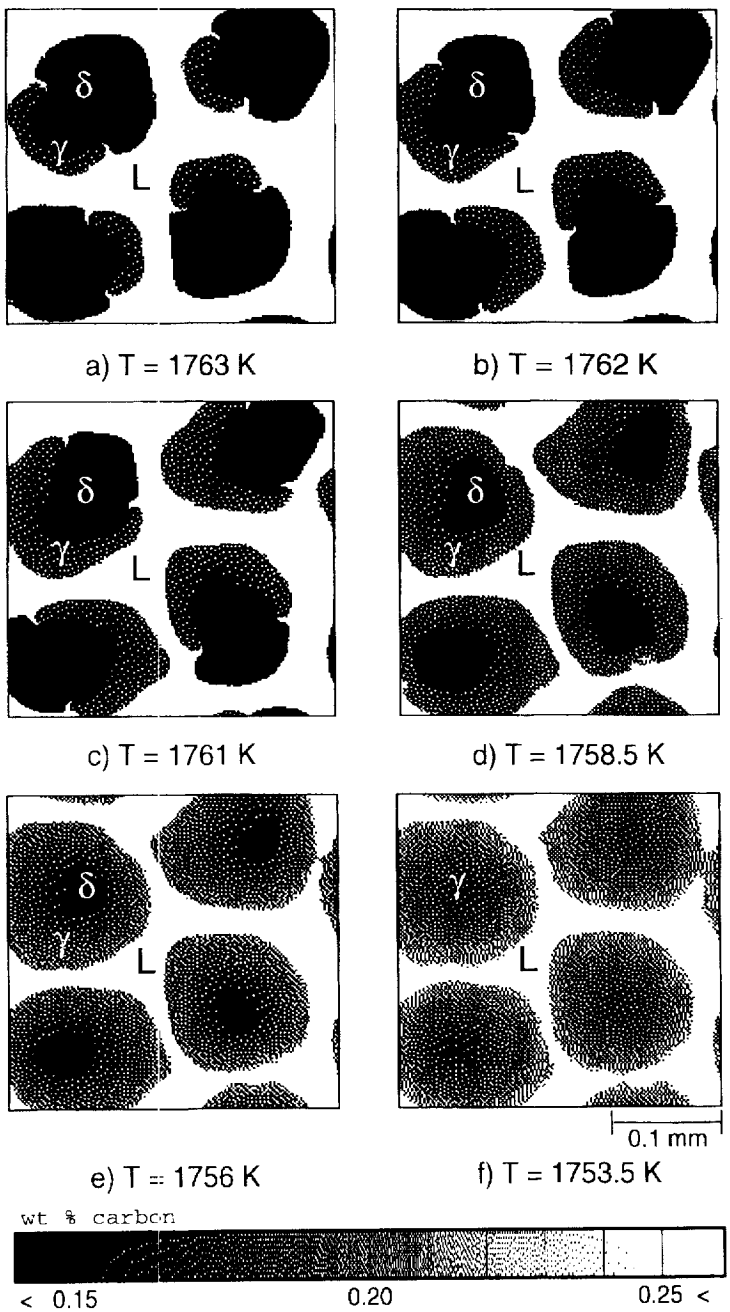

Fig. 5. Simulation of the peritectic solidification in Fe–C. The mixture carbon concentration is illustrated by the grey-scale. The peritectic γ-austenite phase nucleated on the primary properitectic δ-ferrite grows around it by simultaneous consumption of both the ferrite and the liquid phase.

Acknowledgements

We wish to thank Prof. C. Beckermann for helpful discussions about the solute diffusion model. The work was supported partly by the German Bundesministerium für Bildung, Wissenschaft, Forschung und Technologie under grant number 03 K 8002 7 (COST 512) and partly by the Deutsche Forschungsgemeinschaft under grant number SA 335/25-1 (Kurzzeitmetallurgie).

References

[1] I. Steinbach, F. Pezzolla, B. Nestler, J. Rezende, M. Seesselberg, G.J. Schmitz, Physica D 94 (3) (1996) 135.
[2] A.A. Wheeler, W.J. Boettinger, G.B. McFadden, Phys. Rev. A 45 (10) (1992).
[3] L. Bronsard, F. Reitich, Technical Report 92-NA-022, Center of Nonlinear Analysis, Carnegie Mellon University, 1992.
[4] L. Bronsard, H. Garcke, B. Stoth, Proc. Roy. Soc. Edinburgh (1997), submitted.
[5] H. Garcke, B. Nestler, B. Stoth, Physica D 115 (1998) 87–108.
[6] J.B. Collins, H. Levine, Phys. Rev. B 31 (1985) 6119–6122.
[7] G. Caginalp, Arch. Rat. Mech. Anal. 92 (1986) 205.
[8] R. Kobayashi, Physica D 63 (1993) 410–423.
[9] A.A. Wheeler, B.T. Murray, R.J. Schaefer, Physica D 66 (1993) 243–262.
[10] A. Bösch, H. Müller-Krumbhaar, O. Shochet, Z. Phys. B 97 (1995) 367–677.
[11] R. Kobayashi, Experimental Math. 3 (1) (1994).
[12] I. Steinbach, F. Pezzolla, R. Prieler, in: M. Cross, I. Campell (Eds.), Modeling of Casting, Welding and Advanced Solidification Processes VII, TMS (1995) pp. 695–705.
[13] R. Gonzalez-Cinca, L. Ramirez-Piscina, J. Casademunt, A. Hernandez-Machado, L. Kramer, T. Toth Katona, T. Börzsönyi, A. Buke, Physica D 99 (1996) 359–368.
[14] G. Caginalp, W. Xie, Phys. Rev. E 48 (1993) 1897.
[15] H.J. Diepers, C. Beckermann, I. Steinbach, Proceedings of Solidification Processing, Sheffield, 1997.
[16] A.A. Wheeler, W.J. Boettinger, G.B. McFadden, Proc. Roy. Soc. London A 452 (1996) 495.
[17] J.A. Warren, W.J. Boettinger, Acta Metall. Mater. 43 (2) (1995) 689–703.
[18] J. Tiaden, I. Steinbach, Proceedings of the COST 512 Workshop, Davos, 1996.
[19] I. Steinbach, R. Prieler, Transport phenomena in solidification, ASME HTD-284 (1994) 69.
[20] M. Seesselberg, J. Tiaden, G.J. Schmitz, I. Steinbach, Proceedings of Solidification Processing, Sheffield, 1997.